Hollow Cages versus Space-Filling Structures for Medium-Sized Gold Clusters: The Spherical Aromaticity of the Au 50 Cage

ARTICLE *in* THE JOURNAL OF PHYSICAL CHEMISTRY A · NOVEMBER 2005

Impact Factor: 2.69 · DOI: 10.1021/jp052414q · Source: PubMed

Hollow Cages versus Space-Filling Structures for Medium-Sized Gold Clusters: The Spherical Aromaticity of the Au_{50} Cage

Jinlan Wang and Julius Jellinek*

Chemistry Division, Argonne National Laboratory, Argonne, Illinois 60439

Jijun Zhao

Institute for Shock Physics, Washington State University, Pullman, Washington 99164

Zhongfang Chen, R. Bruce King, and Paul von Ragué Schleyer

Department of Chemistry and Center for Computational Chemistry, University of Georgia, Athens, Georgia 30602-2525

Received: May 9, 2005; In Final Form: August 3, 2005

Candidates for the lowest energy structures of medium-sized Au_n, $n = 32$, 38, 44, 50, and 56, clusters were evaluated using gradient-corrected DFT computations. Both hollow cage and space-filling conformations were considered. The cages were constructed using fullerene-based templates. The space-filling structures were generated by employing a genetic algorithm. We have found that the space-filling isomers were lower in energy except for two notable cases. Like Au_{32} [Johansson, M. P.; Sundholm, D.; Vaara, J. *Angew. Chem. Int. Ed.* **2004**, *43*, 2678], a hollow cage configuration of Au_{50} is more stable than its alternative space-filling isomeric forms. The unusual stabilities of the cage Au_{32} and Au_{50} can be attributed to spherical aromaticity; both exhibit large negative nucleus-independent chemical shifts and exceptionally large HOMO−LUMO gaps.

I. Introduction

Gold clusters exhibit remarkable size-specific catalytic activity and selectivity[1,2] and are of potential importance as building units in nanoscale devices.[3−5] The relativistic nature of gold results in unusual structures.[6−28] Most relativistic density functional theory (DFT) computations predicted planar configurations for neutral Au_n up to $n = 11-14$,[6−10] although a recent CCSD(T) treatment[11] questioned some of the DFT findings. Ion mobility and photoelectron spectroscopy experiments confirmed the planar structures of anionic Au_n^- (up to $n = 12$) and cationic Au_n^+ (up to $n = 7$) predicted by DFT computations.[12−14] Three-dimensional space-filling configurations with low symmetry were given by LDA-DFT computations for Au_n clusters in the $n = 15-20$ size range.[8] A beautifully symmetrical Au_{20} (T_d) isomer was identified by a combined photoelectron spectroscopy/GGA-DFT study.[15] The stability of this tetrahedral Au_{20}, which represents a relaxed fragment of the face-centered cubic (fcc) lattice, has been associated with aromaticity.[16]

X-ray powder diffraction studies of gold particles 1−2 nm in diameter (about 40−200 atoms) revealed a truncated decahedral motif.[17,18] Several computational investigations of gold clusters in this size range at different degrees of sophistication favored amorphous space-filling structures.[19−22] In contrast, an icosahedral Au_{32} hollow cage configuration, based on a fullerene template, was recently computed to be especially stable; these unusual geometric and energetic features were attributed to aromaticity.[23] Endohedral structures with 1−3 Au atoms inside the Au_{32} cage were found to be lower in energy than compact configurations for Au_{33-35}.[24] Recently, an icosahedral hollow cage structure of Au_{42}, based on a C_{80} fullerene, was computed to be a local minimum, but it was not as stable as space-filling isomers.[25]

All these findings suggest that hollow cage structures of medium-sized gold clusters may compete with space-filling alternatives. We have explored here this possibility systematically for Au_n, $n = 32$, 38, 44, 50, and 56. These sizes were chosen because of their relationship to fullerenes, as discussed in the next section, which presents the methodological details. The results are discussed in section III. A brief summary is given in section IV.

II. Methodological Details

The reliability of DFT studies depends on the choice of the functional and the basis set for the problem being investigated. We employed the Perdew, Burke, and Ernzerhof[29] (PBE) parametrization of the exchange-correlation functional as well as a DFT-based relativistic semi-core pseudopotential[30] (DSPP), fitted to all-electron relativistic results, and a double numerical basis set including d-polarization functions (DND), as implemented in the DMol package.[31]

The accuracy of the PBE/DSPP/DND combination was evaluated by computations on Au_n, $n = 1-14$ and 20. Table 1 documents the good agreement between the computed results and the available experimental data.[13,15,32−34] In accord with earlier computations,[9,13] we find the transition from 2D to 3D structures to occur at $n = 13$ for anionic gold clusters and at $n = 14$ for neutral Au_n. Our computations also verify the tetrahedral lowest energy structure of Au_{20}. Its HOMO−LUMO gap (1.80 eV) and electron affinity (2.65 eV) are very close to those computed in ref 15 (1.82 and 2.61 eV, respectively; see also Table 1).

Our comparison of stability of hollow cage and space-filling structures of Au_n was performed for sizes n defined by the

* Corresponding author. E-mail: jellinek@anl.gov.

10.1021/jp052414q CCC: $30.25
Published on Web 09/17/2005

TABLE 1: Results of Au_n Computations Using the PBE Functional, DND Basis, and DSPP Pseudopotential (See Text for Details)[a]

system	property	this work	experiment[13,15,32−34]
Au	IP (eV)	9.62	9.23
	EA (eV)	2.07	2.30
Au_2	R_e (Å)	2.56	2.47
	E_b (eV)	1.07	1.15
	IP (eV)	9.43	9.50, 9.22
	EA (eV)	1.82	1.92
Au_3	EA (eV)	3.51	3.88
Au_4	EA (eV)	2.68	2.70
Au_5	EA (eV)	3.01	3.06
Au_6	EA (eV)	2.09	2.06
Au_7	EA (eV)	3.32	3.40
Au_8	EA (eV)	2.80	2.73
Au_9	EA (eV)	3.77	3.81
Au_{10}	EA (eV)	3.06	3.89
Au_{11}	EA (eV)	3.70	3.76
Au_{12}	EA (eV)	3.21	3.03
Au_{13}	EA (eV)	3.88	3.91
Au_{14}	EA (eV)	3.29	2.94
Au_{20}	EA (eV)	2.65	2.73, 2.75

[a] IP is the ionization potential, EA is the electron affinity, and R_e and E_b are the equilibrium bond length and binding energy per atom of Au_2. The EAs are computed as the difference between the total energies of the equilibrated most stable structures of the neutral and anionic forms of the clusters.

TABLE 2: Structure, Symmetry, Binding Energy Per Atom (E_b), Binding Energy Per Atom Corrected by the Zero-Point Energy ($\bar{E}_b$), HOMO−LUMO Gap (Δ), and NICS of the Lowest Energy Cage and Space-Filling Forms for Au_n

system	structure/symmetry	E_b (eV/atom)	$\bar{E}_b$ (eV/atom)	Δ (eV)	NICS (ppm)
Au_{32}	cage/I_h	2.2693	2.2544	1.527	−81.3
	space-filling/C_1	2.2301	2.2168	0.313	
Au_{38}	space-filling/C_1	2.2635	2.2497	0.256	
	cage/D_6	2.2534	2.2388	0.110	(98.8)[a]
Au_{44}	space-filling/C_1	2.2916	2.2780	0.135	
	cage/D_2	2.2901	2.2756	0.173	12.7
Au_{50}	cage/C_2	2.3365	2.3214	0.831	−82.8
	space-filling/C_1	2.3329	2.3188	0.230	
Au_{56}	space-filling/C_1	2.3731	2.3587	0.310	
	cage/C_2	2.3348	2.3195	0.201	−18.3

[a] This large, positive value may be an artifact arising from the exceptionally small HOMO−LUMO gap.

"capping method" used to generate the cages. All possible carbon fullerene isomers[35] for $20 + 2m$ ($m = 0$, 2, 4, 6, and 8) atoms were considered; the carbon atoms were replaced by gold atoms, and an extra gold atoms was added over the center of each pentagonal and hexagonal face. As the total number of faces is $12 + m$, the size of the resulting gold clusters is $n = 32 + 3m$, that is $n = 32$, 38, 44, 50, and 56. The number of cage structures formed in this way for each n is 1, 1, 2, 6, and 15, respectively.[35] Because the length of the Au−Au bond is about twice that of the C−C bond, we rescaled the Cartesian coordinates of all the atoms by a factor of 2 and then performed symmetry-constrained DFT optimizations. This recipe is, of course, not the only way to generate hollow cage structures of clusters. It produces hollow conformations "inspired" by fullerenes.

The space-filling structures of the clusters were generated using a genetic algorithm[36] (GA) with the Gupta-like[37] and Sutton-Chen[38] many-body potentials. Sixteen arbitrary configurations were used as the initial population. Two configurations from this population were chosen randomly as parents to produce an offspring through the mating and mutation procedure. The offspring cluster was then fully relaxed using molecular dynamics and gradient-driven techniques. If the energy of the offspring was lower than that of at least one of the parents, the offspring took the place of the parent with the higher energy. This procedure was repeated until the lowest energy structure in the population remained unchanged in 5000 consecutive iterations. The total number of iterations to achieve this varied between 15 000 and 50 000. Seven to twenty-two low-energy configurations generated in this way for each cluster size were then optimized with DFT. The computed harmonic vibrational frequencies verified that the lowest energy cage and space-filling structures were minima.

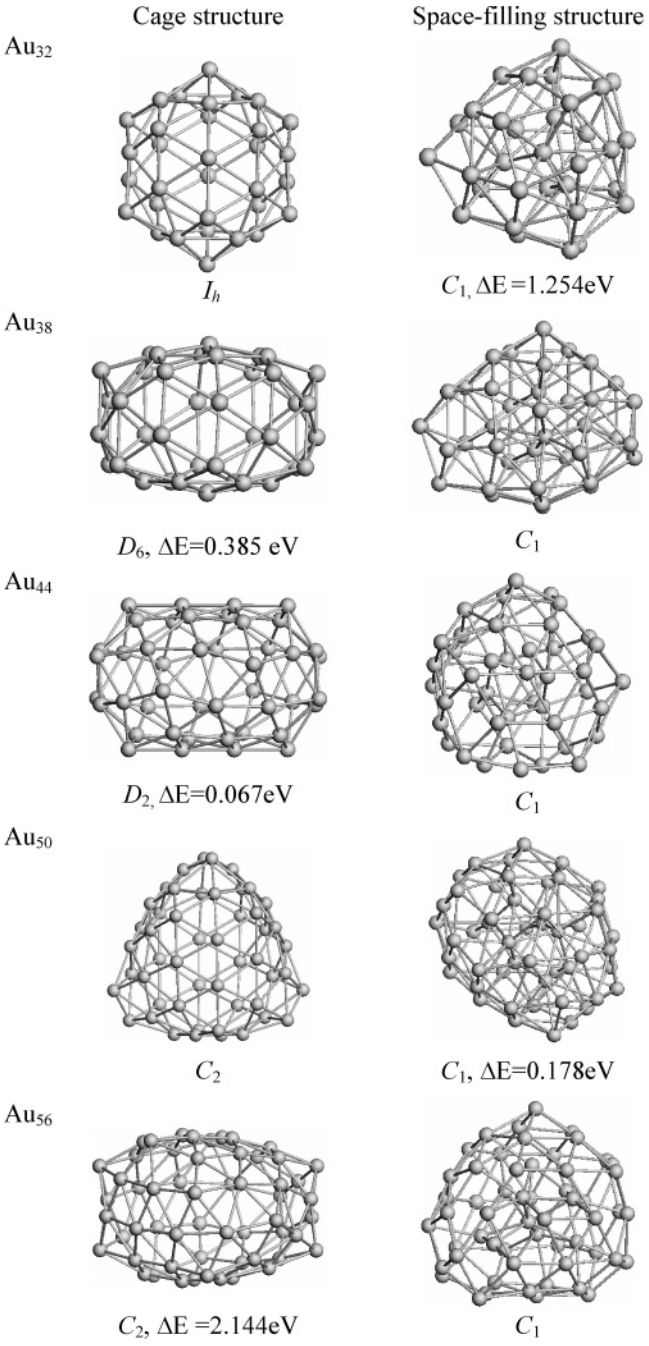

Figure 1. Lowest energy cage and space-filling configurations of Au_n, $n = 32$, 38, 44, 50, and 56. The energy ΔE is referred to the energy of the more stable isomer.

III. Results and Discussion

Structures and Energies. The symmetries, binding energies, and HOMO−LUMO gaps of the lowest energy hollow cage and space-filling configurations of Au_n, $n = 32$, 38, 44, 50,

TABLE 3: Structure, Symmetry ("sym"), and Energy (ΔE) of the Different Isomers of Au_n, $n = 32$, 38, 44, 50, and 56, As Obtained in Our DFT Computations[a]

system	structure	sym	ΔE (eV)	system	structure	sym	ΔE (eV)
Au_{32}	cage	I_h	0.000	Au_{50}	space-filling	C_1	0.932
	space-filling	C_1	1.254		space-filling	C_{2v}	0.954
	space-filling	C_1	1.277		space-filling	C_1	0.977
	space-filling	C_2	1.311		space-filling	C_1	1.084
	space-filling	C_1	1.414		space-filling	C_1	1.124
	space-filling	C_1	1.497		cage	C_2	1.157
	space-filling	C_s	1.576		space-filling	C_1	1.160
	space-filling	C_1	1.584		cage	D_{3d}	1.232
	space-filling	C_1	1.629		space-filling	C_1	1.294
	space-filling	C_2	1.703		space-filling	C_1	1.343
Au_{38}	space-filling	C_1	0.000		cage	D_{3h}	1.433
	space-filling	C_s	0.033		space-filling	C_1	1.446
	space-filling	C_1	0.080		space-filling	C_1	1.548
	cage	D_6	0.385		space-filling	C_1	1.656
	space-filling	C_2	0.446		cage	D_2	1.748
	space-filling	C_{5v}	0.452		space-filling	C_1	1.929
	space-filling	C_1	0.692		space-filling	C_1	2.195
	space-filling	O_h	0.956	Au_{56}	space-filling	C_1	0.000
	space-filling	C_s	1.101		space-filling	C_1	0.331
Au_{44}	space-filling	C_1	0.000		space-filling	C_1	0.357
	cage	D_2	0.067		space-filling	C_1	0.361
	space-filling	C_1	0.387		space-filling	C_1	1.053
	space-filling	C_1	0.422		space-filling	C_1	1.060
	space-filling	C_1	0.473		space-filling	C_{3v}	1.512
	space-filling	C_s	0.498		cage	C_2	2.144
	space-filling	C_1	0.580		cage	C_1	2.273
	space-filling	C_2	0.579		cage	C_2	2.334
	space-filling	C_1	0.874		cage	C_s	2.349
	cage	T_d	0.892		cage	C_1	2.473
Au_{50}	cage	C_2	0.000		cage	D_{3h}	2.531
	space-filling	C_1	0.178		cage	C_{2v}	2.539
	cage	D_3	0.404		cage	D_2	2.555
	space-filling	C_1	0.508		cage	D_{6h}	2.577
	space-filling	C_1	0.614		cage	C_s	2.693
	space-filling	C_1	0.674		cage	D_{2d}	2.798
	space-filling	C_1	0.691		cage	C_2	2.830
	space-filling	C_1	0.760		cage	C_2	2.896
	space-filling	C_1	0.810		cage	D_2	3.010
	space-filling	C_s	0.825		cage	D_{2d}	3.584
	space-filling	C_1	0.883				

[a] Energies are referred to that of the most stable isomer.

and 56, are summarized in Table 2; their structures are depicted in Figure 1. The lowest energy forms of two clusters, Au_{32} and Au_{50}, are hollow cages. The other clusters prefer space-filling isomers as their most stable configurations. In agreement with earlier studies,[23,24] the hollow cage structure of Au_{32} is markedly more stable (by 0.0392 eV/atom, or 0.0376 eV/atom with the zero-point energy correction; see Table 2) than its lowest energy space-filling counterpart. However, the Au_{50} hollow cage wins out over the closest space-filling configuration only by 0.0036 eV/atom, or 0.0026 eV/atom with the zero-point energy correction. The competition is even more pronounced in Au_{44}, where the space-filling form is 0.0015 eV/atom, or 0.0025 eV/atom with the zero-point energy correction, lower in energy. This space-filling preference increases to 0.0101 eV/atom, or 0.0109 eV/atom with the zero-point energy correction, in Au_{38}, and to 0.0383 eV/atom, or 0.0392 eV/atom with the zero-point energy correction, in Au_{56}.

The accuracy of the computations is, of course, a factor in defining the energy ordering of the isomers. The accuracy of our computations is best assessed by comparison with the experimental data presented in section II. In addition, the relative energies of the isomers are, as a rule, reproduced with higher fidelity than their absolute energies. Whereas the preference for the cage structure of Au_{50} may be less clear-cut than in the case of Au_{32}, the high stability and competitiveness of this cage is certainly unusual based on what one might expect for gold clusters of larger sizes.

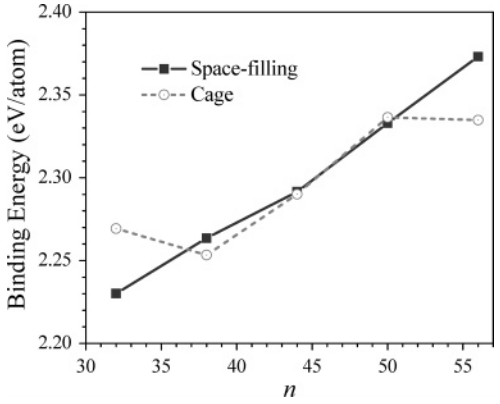

Figure 2. Binding energy per atom as a function of cluster size in the most stable hollow cage (open circles) and space-filling (solid squares) structures of Au_n.

The HOMO−LUMO gap is an additional gauge of the relative stability of the cage and space-filling configurations. This gap for the cage structures of Au_{32} and Au_{50} is substantially larger than not only those of their space-filling isomers (see Table 2) but also those of both forms of Au_{38}, Au_{44}, and Au_{56}. The lower energy, space-filling structures of Au_{38} and Au_{56} possess somewhat larger values. The highly competitive nature of the cage and space-filling configurations of Au_{44} is reflected by the small difference in their HOMO−LUMO gaps; the less stable cage form actually has a slightly larger gap.

Table 3 lists the stationary configurations obtained by our DFT computations. Although we did not compute the vibrational frequencies of all these configurations, at least those with C_1 symmetry should be minima. Consistent with the preference for amorphous packing in Au_n found in earlier studies,[19,20] most of our low-energy space-filling structures have C_1 symmetry. With the exception of Au_{38}, the cage forms of the clusters were optimized under the symmetry of the fullerene templates from which they were generated. For the Au_{38} cage, the D_{6d} symmetry of the underlying 24-atom fullerene leads to HOMO−LUMO degeneracy. The Jahn−Teller effect lowers the symmetry of Au_{38} to D_6.

Aromaticity and NICS Analysis. Why are certain hollow cage structures of medium-sized gold clusters preferred? Can one predict when a hollow cage form of a given Au_n will be more stable than its space-filling competitors? The aromaticity concept helps answer these questions; it was invoked to explain the tetrahedral structure of Au_{20}[16] and the preference for hollow cage in Au_{32}.[23] Aromaticity is associated with extra stability arising from electron delocalization in complete circuits as are found in annulene rings and three-dimensional molecules.[39] Magnetic properties, such as the nucleus-independent chemical shifts (NICS),[40] may be used as quantitative measures of aromaticity. We computed NICS at the centers of the lowest energy hollow cage Au_n structures (see Table 1) using the PBE functional and the LANL2DZ basis set[41] as implemented in the Gaussian-98 package.[42] Test computations validated the change from the DND/DSPP (DMol) to the LANL2DZ (Gaussian) level (program).[43]

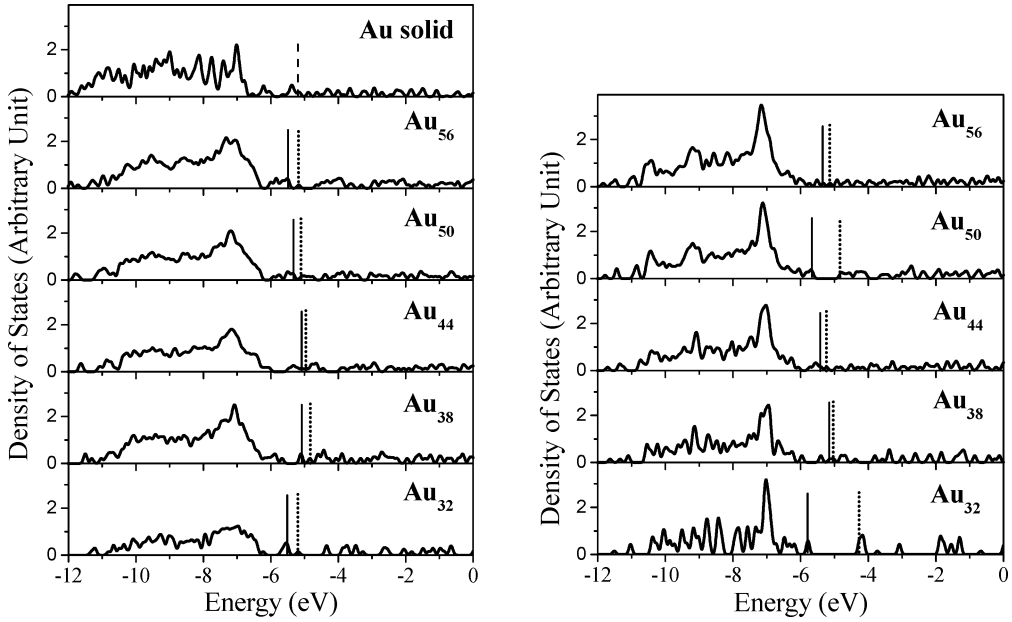

Figure 3. Electron densitities of states of the space-filling structures (left panels) and cage structures (right panels) of the Au_n, $n = 32$, 38, 44, 50, and 56, clusters. For comparison the DOS of the fcc bulk gold is also shown. A Gaussian full width at half-height broadening of 0.05 eV is used around each computed eigenenergy. The solid vertical lines correspond to HOMO, the dotted to LUMO, and the dashed to the Fermi level of the bulk gold.

As judged by their highly negative (diatropic) NICS values (ca. −82 ppm, Table 2), the cage structures of Au_{32} and Au_{50} are strongly aromatic. In contrast, the hollow cage structures of the other clusters, which are less stable than their space-filling counterparts are, at best, rather weakly aromatic (Au_{56}, NICS = −18.3) or even antiaromatic (Au_{38} and Au_{44}). Interestingly, the $2(k + 1)^2$ skeletal electron counting rule,[16,44] as an indicator of spherical aromaticity, applies to both Au_{32}[23] and Au_{50} if one makes the assumption that each Au atom contributes to bonding only one (6s) valence electron. With this assumption, Au_{32} and Au_{50} possess the necessary "magic number" of skeletal electrons: 32 with $k = 3$ and 50 with $k = 4$, respectively. However, the assumption that only a single electron per Au atom is involved is an oversimplification, because electrons in d orbitals also contribute to bonding in gold clusters; alkali metal clusters behave differently. More detailed reasons for the apparent applicability of the $2(k + 1)^2$ rule to hollow cage gold clusters are under investigation by our research groups.

Density of States. Density of states (DOS) graphs based on our computations are presented in Figure 3 for the lowest energy space-filling and hollow cage structures of Au_n, $n = 32$, 38, 44, 50, and 56. The DOS of fcc bulk gold also is shown for comparison. Both common and dissimilar features are evident. The overall range of relevant energies and the peak at or around 7 eV are common to all the DOS plots. Due to their lower symmetry, the DOSs of the space-filling isomers are broader than those of their higher-symmetry hollow cage counterparts. The high (I_h) symmetry of Au_{32} results in particularly well-resolved DOS peaks. The symmetry argument also explains the well-resolved fcc bulk gold DOS graph.

The large HOMO−LUMO gaps of the hollow cage Au_{32} and Au_{50} isomers are among the most notable features discernible in Figure 3. In contrast, the space-filling Au_{32} and Au_{50} isomers, as well as all the other clusters, have relatively small HOMO−LUMO gaps. The large gaps of the Au_{32} and Au_{50} hollow cages as well as their large negative NICS values reflect and help rationalize their extra stability.

We complete the above analysis with the following cautionary remarks. The value of NICS alone may not be an unambiguous indicator of cluster stability. As mentioned, NICS is a measure of the degree of electron delocalization in closed circuits—the basis of aromaticity. However, the extra stabilization associated with aromaticity usually accounts for only 5−10% of the total binding energy. Although this contribution is important, and often decisive, the usual bonding considerations (e.g., close packing) may dominate. NICS also is not free from the contributions of local effects of the individual skeletal bonds and the molecular symmetry may be important. Indeed, the moduli of large negative NICS values of different isomers may not necessarily correlate with their relative energies. The data in Table 4 for the cage forms of Au_{50} are instructive and suggest a relationship with symmetry. None of the cage forms of Au_{50} have the highest possible symmetry, but all follow the $2(k + 1)^2$ rule, as discussed above. This rule is based on the spherical symmetry, which molecules can only approach. Although the D_3 Au_{50} isomer is not the most stable, it has the highest symmetry and the most negative NICS. The NICS values of the two lower symmetry C_2 isomers are smaller in magnitude, but individually are in line with their relative energies. The main point is that the NICS of all these A_{50} isomers are large and negative.

TABLE 4: Symmetry, Energy (ΔE), HOMO−LUMO Gap (Δ), NICS, and the Lowest Vibrational Frequency (ν_{min}) of the First Three Cage Isomers of Au_{50}

structure	symmetry	ΔE (eV)	Δ (eV)	NICS (ppm)	ν_{min} (cm^{-1})
cage[a]	C_2	0.000	0.831	−82.8	20.7
cage	D_3	0.404	0.793	−90.0	20.4
cage	C_2	1.157	0.167	−79.2	18.7

[a] The configuration of the frontier orbitals of this cage structure is $(b)^2(a)^2(a)^0$.

The HOMO−LUMO gap (Table 4) of the most stable Au_{50} isomer is the largest. It is followed closely by the value for the second cage structure, which is the third isomer of Au_{50} in Table 3, and the considerably smaller value for the third cage structure, which is the seventeenth isomer of Au_{50} in Table 3. Along with the relative energies, judicious evaluation of the NICSs and the

HOMO−LUMO gaps may help identify and characterize the most stable isomeric form more completely than either of these quantities alone.

IV. Summary

Structures of medium-sized Au_n clusters have been surveyed using gradient-corrected density functional theory. Hollow cage configurations can compete energetically with their space-filling counterparts. In particular, Au_{50}, like Au_{32} considered earlier, favors a fullerene-based cage structure. The extra stabilities of the hollow cage forms of both Au_{32} and Au_{50} correlate with their large HOMO−LUMO gaps and large negative NICS values. The latter indicate that spherical aromaticity may be responsible for the extra stability of the hollow cage configurations of certain cluster sizes. In contrast, the icosahedral Au_{42} hollow cage does not follow the $2(k + 1)^2$ rule, and has been reported recently[25] not to be aromatic and to be higher in energy than its space-filling isomers.

The technological potential of nanosized stable hollow cages is quite diverse. For example, they may be used to encapsulate atoms, molecules, or other clusters,to be incorporated themselves inside carbon nanotubes,[45] and to be utilized as contacts between organic molecules in molecular electronic devices.

Acknowledgment. J.W. thanks Dr. T. X. Li for providing coordinates of some structures. This work was supported by the Office of Basic Energy Sciences, Division of Chemical Sciences, Geosciences, and Biosciences, U.S. Department of Energy, under Contract number W-31-109-Eng-38 (J.J. and J.W.), and by NSF Grant CHE-0209857 (R.B.K., P.R.S., and Z.C.).

Note Added after ASAP Publication. This article was published ASAP on September 17, 2005. Two values in Table 2 have been changed. The correct version was posted on September 21, 2005.

References and Notes

(1) Haruta, M.; Kobayashi, T.; Sano, H.; Yamada, N. *Chem. Lett.* **1987**, *2*, 405.
(2) Bond, G. C.; Thompson, D. T. *Gold Bull.* **2000**, *33*, 41.
(3) Schwerdtfeger, P. *Angew. Chem., Int. Ed.* **2003**, *42*, 1892.
(4) Pyykkö, P. *Angew. Chem., Int. Ed.* **2004**, *43*, 4412.
(5) Daniel, M. C.; Astruc, D. *Chem. Rev.* **2004**, *104*, 293.
(6) Hakkinen, H.; Landman, U. *Phys. Rev. B* **2000**, *62*, 2287.
(7) Bonacic-Koutecky, V.; Burda, J.; Mitric, R.; Ge, M. F.; Zampella, G.; Fantucci, P. *J. Chem. Phys.* **2002**, *117*, 3120.
(8) Wang, J. L.; Wang, G. H.; Zhao, J. J. *Phys. Rev. B* **2002**, *66*, 035418.
(9) Xiao L.; Wang, L. C. *Chem. Phys. Lett.* **2004**, *392*, 452.
(10) Fernandez, E. M.; Soler, J. M.; Garzon, I. L.; Balbas, L. C. *Phys. Rev. B* **2004**, *70*, 165403.
(11) Olson, R. M., Varganov, S. Gordon, M. S., Metiu, H., Chretien, S., Piecuch, P., Kowalski, K., Kucharski, S. A., Musial, M. *J. Am. Chem. Soc.* **2005**, *127*, 1049.
(12) Furche, F.; Ahlrichs, R.; Weis, P.; Jacob, C.; Gilb, S.; Bierweiler, T.; Kappes, M. M. *J. Chem. Phys.* **2002**, *117*, 6982.
(13) Hakkinen, H.; Yoon, B.; Landman, U.; Li, X.; Zhai, H. J.; Wang, L. S. *J. Phys. Chem. A* **2003**, *107*, 6168.
(14) Gilb, S.; Weis, P.; Furche, F.; Ahlrichs, R.; Kappes, M. M *J. Chem. Phys.* **2002**, *116*, 4094.
(15) Li, J.; Li, X.; Zhai, H.-J.; Wang, L.-S. *Science* **2003**, *299*, 864.
(16) King, R. B.; Chen, Z.; Schleyer, P. v. R. *Inorg. Chem.* **2004**, *43*, 4564.
(17) Cleveland, C. L.; Landman, U.; Schaaff, T. G.; Shafigullin, M. N.; Stephens, P. W.; Whetten, R. L. *Phys. Rev. Lett.* **1997**, *79*, 1873.
(18) Schaaff, T. G.; Shafigullin, M. N.; Khoury, J. T.; Vezmar, I.; Whetten, R. L.; Cullen, W. G.; First, P. N.; Gutierrez-Wing, C.; Ascensio, J.; Jose-Yacaman, M. J. *J. Phys. Chem. B* **1997**, *101*, 7885.
(19) Garzon, I. L.; Michaelian, K.; Beltran, M. R.; Posada-Amarillas, A.; Ordejon, P.; Artacho, E.; Sanchez-Portal, D.; Soler, J. M. *Phys. Rev. Lett.* **1998**, *81*, 1600.
(20) Michaelian, K.; Rendon, N.; Garzon, I. L. *Phys. Rev. B* **1999**, *60*, 2000.
(21) Doye, J. P. K.; Wales, D. J. *New J. Chem.* **1998**, *22*, 733.
(22) Li, T. X.; Yin, S. Y.; Ji, Y. L.; Wang, B. L.; Wang, G. H.; Zhao, J. *Phys. Lett. A* **2000**, *267*, 403.
(23) Johansson, M. P.; Sundholm, D.; Vaara, J. *Angew. Chem., Int. Ed.* **2004**, *43*, 2678.
(24) Gu, X.; Ji, M.; Wei, S. H.; Gong, X. G. *Phys. Rev. B*, **2004**, *70*, 205401.
(25) Gao, Y.; Zeng, X. C. *J. Am. Chem. Soc*. **2005**, *127*, 3698**.**
(26) Wang, J. L.; Wang, G. H.; Zhao, J. J. *Chem. Phys. Lett.* **2003**, *380*, 716.
(27) (a) Remacle, F.; Kryachko, E. S. *Advances in Quantum Chemistry*; Elsevier: New York, 2004; Vol. 47, pp 423−464. (b) Remacle, F.; Kryachko, E. S. *J. Chem. Phys*. **2005**, *122*, 044304.
(28) (a) Kondo, Y.; Takayanagi, K. *Science* **2000**, *289*, 606. (b) Wang, B. L.; Yin, S. Y.; Wang, G. H.; Buldum, A.; Zhao, J. J. *Phys. Rev. Lett.* **2001**, *86*, 2046. (c) Oshima, Y.; Onga A.; Takayanagi, K. *Phys. Rev. Lett.* **2003**, *91*, 205503.
(29) Perdew, J. P.; Burke, K.; Ernzerhof, M. *Phys. Rev. Lett.* **1996**, *77*, 3865.
(30) Delley, B. *Phys. Rev. B* **2002**, *66*, 155125.
(31) DMOL is a density functional theory program distributed by Accelrys, Inc. Delley, B. *J. Chem. Phys.* **1990**, *92*, 508; *J. Chem. Phys.* **2000**, *113*, 7756.
(32) *NIST Standard Reference Database 69−March 2003 Release: NIST Chemistry WebBook*; http://webbook.nist.gov.
(33) James, A. M.; Kowalczyk, P.; Simard, B.; Pinegar, J. C.; Morse, M. D. *J. Mol. Spectrosc.* **1994**, *168*, 248.
(34) Morse, M. D. *Chem. Rev*. **1986**, *86*, 1049.
(35) Fowler, P. W.; Manolopoulos, D. E.; Ryan, R. P. In *The Fullerenes*; Kroto, H. W., Fischer, J. E., Cox, D. E., Eds.; Pergamon: Oxford, U.K., 1993.
(36) Deaven, D. M.; Ho, K. M. *Phys. Rev. Lett.* **1995**, *75*, 288.
(37) (a) Gupta, R. P. *Phys. Rev. B* **1989**, *23*, 6265. (b) Cleri, F.; Rosato, V. *Phys. Rev. B* **1993**, *48*, 22. (c) Lopez, M. J.; Jellinek, J. *J. Chem. Phys.* **1999**, *110*, 8899.
(38) Sutten, A. P.; Chen, J. *Philos. Mag. Lett.* **1990**, *61*, 139.
(39) Schleyer, P. v. R., Ed. Special Issue on Aromaticity. *Chem. Rev.* **2001**, *101*, 1115ff.
(40) (a) Schleyer, P. v. R.; Maerker, C.; Dransfeld, A.; Jiao, H.; Hommes, N. J. R. v. E. *J. Am. Chem. Soc.* **1996**, *118*, 6317. (b) Chen, Z.; Heine, T.; Schleyer, P. v. R.; Sundholm, D. In *Calculation of NMR and EPR Parameters. Theory and Applications*; Kaupp, M., Bûhl, M., Malkin, V. G., Eds.; Wiley-VCH Verlag GmbH & Co. KGaA: Weinheim, 2004.
(41) Hay, P. J.; Wadt, W. R. *J. Chem. Phys.* **1985**, *82*, 270; 284; 299.
(42) Frisch, M. J.; Trucks, G. W.; Schlegel, H. B.; Scuseria, G. E.; Robb, M. A.; Cheeseman, J. R.; Montgomery, J. A., Jr.; Vreven, T.; Kudin, K. N.; Burant, J. C.; Millam, J. M.; Iyengar, S. S.; Tomasi, J.; Barone, V.; Mennucci, B.; Cossi, M.; Scalmani, G.; Rega, N.; Petersson, G. A.; Nakatsuji, H.; Hada, M.; Ehara, M.; Toyota, K.; Fukuda, R.; Hasegawa, J.; Ishida, M.; Nakajima, T.; Honda, Y.; Kitao, O.; Nakai, H.; Klene, M.; Li, X.; Knox, J. E.; Hratchian, H. P.; Cross, J. B.; Adamo, C.; Jaramillo, J.; Gomperts, R.; Stratmann, R. E.; Yazyev, O.; Austin, A. J.; Cammi, R.; Pomelli, C.; Ochterski, J. W.; Ayala, P. Y.; Morokuma, K.; Voth, G. A.; Salvador, P.; Dannenberg, J. J.; Zakrzewski, V. G.; Dapprich, S.; Daniels, A. D.; Strain, M. C.; Farkas, O.; Malick, D. K.; Rabuck, A. D.; Raghavachari, K.; Foresman, J. B.; Ortiz, J. V.; Cui, Q.; Baboul, A. G.; Clifford, S.; Cioslowski, J.; Stefanov, B. B.; Liu, G.; Liashenko, A.; Piskorz, P.; Komaromi, I.; Martin, R. L.; Fox, D. J.; Keith, T.; Al-Laham, M. A.; Peng, C. Y.; Nanayakkara, A.; Challacombe, M.; Gill, P. M. W.; Johnson, B.; Chen, W.; Wong, M. W.; Gonzalez, C.; Pople, J. *Gaussian 98*; Gaussian, Inc.: Pittsburgh, PA, 1998.
(43) The use of the LANL2DZ basis set as implemented in the Gaussian package for evaluating NICS justified by our test calculations on the Au atom, Au_2 diatomic, as well as the Au_{32} and Au_{50} cages. The DND/DSPP-DMol and the LANL2DZ-Gaussian give nearly the same geometric parameters (e.g., bond lengths within ~0.01 Å) and relative energies (within 0.03 eV) for both Au_{32} and Au_{50}. The ionization potential (9.52 eV) and the electron affinity (2.26 eV) of the Au atom as well as the equilibrium binding energy (2.17 eV) and bond length (2.55 Å) of Au_2 obtained with the Gaussian agree well with experimental and Dmol results (Table 1). In addition, our large NICS (−81.3) for Au_{32} cage corresponds to the −100 value obtained recently at a different theoretical level.[23]
(44) Hirsch, A.; Chen, Z. F.; Jiao, H. *Angew. Chem., Int. Ed.* **2000**, *39*, 3915.
(45) Zhao, J.; Wen, B.; Zhou, Z.; Chen, Z.; Schleyer, P. v. R. *Phys. Rev. B*, submitted for publication.